



Heat transfer enhancement by nanofluid coupling with surfactant in overcoming particle agglomeration for microchannel heat sinks

Mohamad Nur Hidayat Mat¹ · R. Saidur^{2,3}

Received: 22 March 2022 / Accepted: 14 July 2022 / Published online: 3 August 2022
© The Author(s), under exclusive licence to Springer-Verlag GmbH Germany, part of Springer Nature 2022

Abstract

The characteristic effect of nanoparticles, boron nitride nanotubes in the nanofluid with and without surfactant, were investigated using numerical CFD. A simplified microchannel heat sink model was created and discretized for numerical analysis. The numerical prediction was validated with previous experiment data for promising numerical agreement. Then, the effect of different Triton X-100 surfactant volume fractions and nanotube mass fractions in the base fluid were carried out on thermal and hydraulic performance. The significant finding revealed that the thermal resistance was reduced by as much as 90% compared to pure water with a surfactant concentration of 0.35 vol.% and adding 0.02 wt.% at the Reynolds number (Re) of 400. However, the Nusselt number (Nu) increased twice from the pure water with an additional surfactant of 0.35 vol.% after the Re of 400. Despite improving the thermal performance, the pressure drop seems to be a drawback for the nanotube with surfactant implementation. The present study resulted in a greater comprehension of the nanofluid flow with surfactant effect in the nanofluid in the microchannel heat sink, allowing for better design decisions to be made for the improvement of this application for various purposes.

Keywords Microchannel heat sink · Numerical · Nanofluid · Nanotube · Surfactant

List of symbols

c_p	Specific heat, J kg ⁻¹ K ⁻¹
$c_{p\text{bf}}$	Specific heat of base fluid, J kg ⁻¹ K ⁻¹
D	Diameter, m
h	Heat transfer coefficient, W m ⁻² K ⁻¹
k	Thermal conductivity, W m ⁻¹ K ⁻¹
k_{bf}	Thermal conductivity of the base fluid, W m ⁻¹ K ⁻¹
k_{Brownian}	Brownian, W m ⁻¹ K ⁻¹
k_{eff}	Effective thermal conductivity of Brownian
k_{static}	Static thermal conductivity, W m ⁻¹ K ⁻¹
Nu	Nusselt number
P	Pressure, Pa

q	Heat flux, W m ⁻²
R	Thermal resistance, m ² K W ⁻¹
Re	Reynolds number
T	Temperature, K
v	Velocity, m s ⁻¹
W	Pumping power, W
μ	Dynamic viscosity, Pa s
μ_{eff}	Effective dynamic viscosity, Pa s
μ_{static}	Static dynamic viscosity, Pa s
μ_{Brownian}	Brownian dynamic viscosity, Pa s
μ_{bf}	Dynamic viscosity of the base fluid, Pa s
ρ	Density, kg m ⁻³
ρ_{bf}	Density of the base fluid, kg m ⁻³
vol	Nanoparticle volume fraction, %

✉ Mohamad Nur Hidayat Mat
mn.hidayat@utm.my

¹ School of Mechanical Engineering, Faculty of Engineering, Universiti Teknologi Malaysia, 81310 UTM Johor Bahru, Malaysia

² Research Centre for Nano-Materials and Energy Technology (RCNMET), School of Engineering and Technology, Sunway University, No. 5, Jalan Universiti, Bandar Sunway, 47500 Petaling Jaya, Selangor Darul Ehsan, Malaysia

³ School of Engineering, Lancaster University, Lancaster LA1 4YW, UK

Subscripts

α	Channel aspect ratio
β	Wall width ratio
W	Heat sink width, cm
L	Heat sink length, cm
t	Substrate thickness, mm
H_c	Channel height, mm

1 Introduction

A microchannel heat sink (MCHS) is an advanced cooling technique that removes excess heat from electrical and electronic device components through a cooling medium (Zhou et al. 2020). The cooling medium is made of distilled water as a heat transfer carrier. Due to the fourth industrialization, this standalone distilled water in MCHS has its limitation of dissipating a large amount of heat flux from a small area (Drummond et al. 2018; Monavari et al. 2021). Therefore, nanoparticles have been added to aid in the heat transfer process, and they continue to be a topic of interest in recent years.

Several techniques have been proposed to enhance the performance of MCHS, including the use of various cooling fluids (Bahiraei et al. 2021; Chuan et al. 2015; Xia et al. 2015), different rib channels (Ghani et al. 2017; Japar et al. 2018), introduce channel porosity (Gong et al. 2018), adding several fins (Fisher and Torrance 2001; Knight et al. 1992; Wei and Joshi 2003), and apply different channel geometries (Alhamid et al. 2019; Ardiansyah et al. 2019; Bahiraei et al. 2019; Bahiraei and Monavari 2020; Monavari et al. 2021; Weisberg et al. 1992). Among these techniques, adding nanoparticles to the base fluid is the most straightforward and effective. Compared to fabricating a new geometry, this method is simple, inexpensive, and straightforward to implement. However, a large number of nanoparticles would cause particle instability, leading to particle agglomeration in the channel (Heidarshenas et al. 2021).

Several methods have been used to attain the stability of the nanotubes. These methods include sonification, high shear, high-pressure homogenization, controlling pH value, surfactant, surface modification technique, and ball milling (Dey et al. 2017). The addition of surfactant to the nanofluid is one of the simplest and most cost-effective ways to increase the nanotubes' stability. The surfactant may be anionic, cationic, or anionic, such as Sodium dodecyl sulfate (SDS) and polyvinyl pyrrolidone (PVP). These surfactants act as a stabilizing agent for the nanoparticles in the nanofluid by reducing the interfacial tension between nanoparticles (Babu et al. 2017). Based on the effectiveness, a study was conducted using 0.01% surfactant with TiO₂ nanofluids, and the thermal conductivity increased by 33% when using 5% nanotubes (Murshed et al. 2005). The dispersion stability of Al₂O₃ nanotubes in nanofluid with and without surfactant was investigated. This study discovered that the nanoparticles' dispersion increased as the nanofluid's surfactant concentration rose (Li et al. 2008). Besides, an investigation of copper-ethylene glycol nanofluid with PVP surfactant concluded that the stability of the nanotubes could be improved by adding the surfactant (Yu et al. 2010).

Triton X-100 has been used as a surfactant for heat transfer improvement in the nanofluid. An experimental study reported that TX-100 at 30 °C improved MCHS's thermal capability even without nanoparticles (Shamsuddin et al. 2021). An experimental study of thermosyphon heat pipe uses TX-100 as a surfactant. They reported combining TX-100 with boron nitride nanoparticles (BNNTs) in nanofluid resulting in lower thermal resistance and higher thermal efficiency of the heat pipe system (Ghorabae et al. 2020). According to another study, the heat pipe's efficiency could be increased by up to 20.9% by adding approximately 2% of TX-100's concentration. The application of TX-100 also has been reported to be used in a solar collector. The result described that additional TX-100 in the nanofluid that contains TiO₂ nanotubes provided excellent performance than water (Kiliç et al. 2018). In addition, Triton TX-100 significantly impacted the suspension stability and sunlight absorption characteristics of multi-walled carbon nanotubes in nanofluid to improve solar thermal absorption (Choi et al. 2018). Despite the benefits of the surfactants, significant limitations and adverse effects of surfactants have been recorded so far, such as foam foaming at high temperatures. This effect may degrade the thermal performance of the fluid flow (Dey et al. 2017). Therefore, to the best of our knowledge, no work has been published on the combined effect of Triton X-100 as a surfactant and the nanoparticle BNNT for Microchannel heat sink using the numerical CFD approach. Thus, this research is focused on closing this gap.

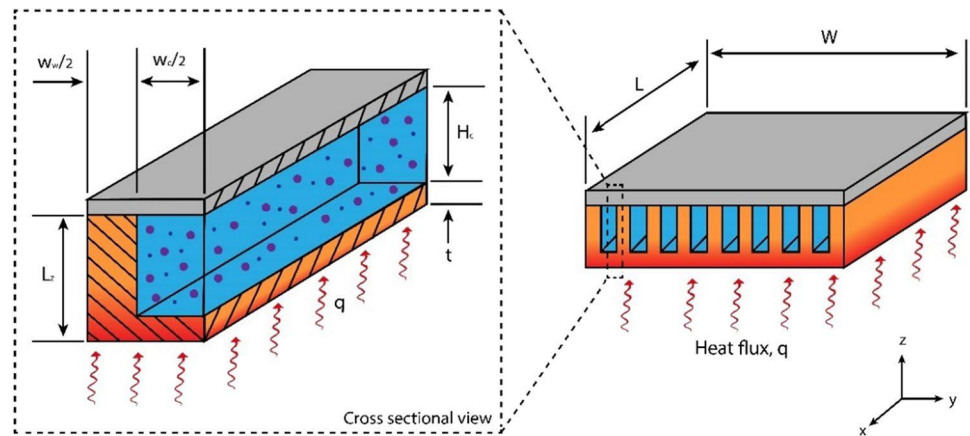
This study used numerical CFD to investigate the effect of adding TX-100 surfactant to boron nitride nanoparticles. This approach can clarify the complex flow and heat transfer patterns inside MCHS with much more detail and reduce cost. To clearly understand the effect of this additional surfactant, three (3) different fluids were created: distilled water alone, TX-100 mixing with distilled water, and TX-100 mixing with BNNT nanoparticle in distilled water. These categories of fluid were simulated against Reynold's number and temperature. For this research, the presentation of the characteristic effect of heat transfer in terms of thermal resistance, Nusselt number, and pressure drop in contour plots would be a novelty for this research.

The paper is organized as follows, the definition of different fluids used is presented in Sect. 2, and geometrical parameters are described in the problem statement. The governing equation described the equation used in the CFD study is shown in Sect. 2, and the definition of performance indicators is in Sect. 2.4. Validation study through grid-independent tests as detailed in Sect. 2.8. Finally, the result and discussion in Sect. 3 and the conclusion appeared in the last section.

Table 1 Nanofluid variable

Fluid	Definition of variable
Nanofluid with surfactant	Varying surfactant volume fraction: 0.005 to 0.035 vol.%, (increment 0.005 vol.%) Fix parameter: 0.001 wt.% of nanotubes in the base fluid and 5 nm of nanotube diameter
Nanofluid with nanotubes mass fraction	Varying nanotube mass fraction: 0.005 to 0.02 wt.% (Increment 0.005 wt.%) Fix parameter: 0.35 vol.% of surfactant in the base fluid and 5 nm of nanotube diameter
Nanofluid with nanotube size	Varying nanotube diameter: 5, 100, 200, and 300 nm Fix parameter: 0.35 vol.% of surfactant in the base fluid and 5 nm of nanotube diameter

Fig. 1 Simplified microchannel heat sink model



2 Methodology

2.1 Concentration of fluid

The heat transfer effect and the pressure drop of a microchannel heat sink were investigated at different concentrations of Triton TX-100 surfactant ranging from 0.005 to 0.035 vol.% with an increment of 0.005 vol.%. The different ranges of BNNTs' mass fractions range from 0.005 to 0.02 wt.% with an increment of 0.005 wt.% were used in this study. Besides, different nanoparticle diameters ranging from 5, 100, 200, and 300 nm against pure water as presented in Table 1. While simulating those variables, some parameters must keep constant such as the volume fraction of 0.35 vol.%, mass fraction of nanotube 0.001 wt.% and 5 nm of nanotube diameter. These fixed parameters were used based on a previous reference study using the same nanotube and surfactant type (Shamsuddin et al. 2021). Based on a previous study on the use of Boron nitrate nanotubes with surfactant for thermal conductivity effect, the range of volume fraction, mass fraction, and nanotube diameter was chosen (Gómez-Villarejo et al. 2019). Consequently, the current result can be related to and compared with the previous finding on the same variable range for thermal and hydraulic performance.

2.2 Computational domain

Since the model employed numerical analysis, this analysis began with the creation of 3D geometry. The geometry was created using computer-aided design to represent the numerical computational domain. The dimension of channels is 10 mm × 10 mm × 0.213 mm (length, $L \times$ width, $W \times$ substrate, t) as demonstrated in Fig. 1 and the dimension presented in Table 2. The material assigned to this channel was silicon rubber, as proposed by previous literature (Tuckerman and Pease 1981). As Husain and Kim (2008) proposed, this analysis only considered a single symmetrical channel. This simplified model was employed because its effect on the opposite side of the domain is symmetrical.

Table 2 Design variable and constrain

Design variables	Value
Channel aspect ratio, α	5.218
Wall width ratio, β	1.0
Heat sink width, W (cm)	1.0
Heat sink length, L (cm)	1.0
Substrate thickness, t (mm)	0.0213
Channel height, H_c (mm)	0.032

Consequently, the model can lessen the computational load and time required for numerical simulation. Upon successfully obtaining optimum mesh size or suitable representative cell length, CFD analysis proceed with α and β so that this analysis can be made comparable with previous study.

2.3 Thermophysical properties of the nanofluid

To reduce computational load, few assumptions were made about the fluid property acting as a single-phase and homogeneous flow between the base fluid and the nanoparticle in this study. Therefore, the nanofluid's properties depend on the base fluid's temperature, as shown below (Alfaryjat et al. 2018; Ghasemi and Aminossadati 2010):

$$\rho_{bf} = \frac{999.84 + 18.225(T + 273.15) - 7.92 \times 10^{-3}(T + 273.15)^2 - 5.545 \times 10^{-5}(T + 273.15)^3 + 1.498 \times 10^{-7}(T + 273.15)^4 - 3.933 \times 10^{-10}(T + 273.15)^5}{1 + 1.816 \times 10^{-2}(T + 273.15)}, \tag{1}$$

$$\mu_{bf} = 2.414 \times 10^{-5} \times 10^{\frac{247.8}{T-140}}, \tag{2}$$

$$Cp_{bf} = 8958.9 - 40.535T + 0.11243T^2 - 1.014 \times 10^{-4}T^3, \tag{3}$$

$$k_{bf} = -0.58166 + 6.3556 \times 10^{-3}T - 7.964 \times 10^{-6}T^2. \tag{4}$$

In the present study, boron nitride nanotube (BNNT) was used as a nanoparticle because its good thermal conductivity and properties are comparable to carbon nanotube (CNT). Therefore, the thermophysical properties of the nanofluid depend on the nanotube volume fraction, ϕ . The properties can be obtained using the equation below (Alfaryjat et al. 2018):

$$\rho_{nf} = (1 - \phi)\rho_{bf} + \phi\rho_{np}, \tag{5}$$

$$\rho_{nf}Cp_{nf} = (1 - \phi) \cdot \rho_{bf}Cp_{bf} + \phi\rho_{np}Cp_{np}. \tag{6}$$

The thermal conductivity can be calculated using empirical correlation of Brownian motion as given below:

$$k_{eff} = k_{static} + k_{Brownian}. \tag{7}$$

The static thermal conductivity is given by:

$$k_{static} = k_{bf} \left[\frac{k_{np} + 2k_{bf} - 2(k_{bf} - k_{np})\phi}{k_{np} + 2k_{bf} + (k_{bf} - k_{np})\phi} \right]. \tag{8}$$

The Brownian thermal conductivity is given as:

$$k_{Brownian} = 5 \times 10^4 \beta \cdot \phi \cdot \rho_{bf} \cdot Cp_{bf} \sqrt{\frac{\sigma_B \cdot T}{\rho_{np} \cdot d_{np}}} \cdot f(T, \phi), \tag{9}$$

$$f(T, \phi) = (2.8217 \times 10^{-2} \cdot \phi + 3.917 \times 10^{-3} \left(\frac{T}{T_o} \right) + (-3.0699 \times 10^{-2} \cdot \phi - 3.91123 \times 10^{-3})). \tag{10}$$

The Boltzmann constant is represented by σ_B and β is the fraction of fluid volume fraction with moving nanoparticles:

$$\mu_{eff} = \mu_{static} + \mu_{brownian}, \tag{11}$$

$$\mu_{static} = \frac{\mu_{bf}}{(1 - \phi)^{2.5}}, \tag{12}$$

$$\mu_{Brownian} = 5 \times 10^4 \beta \cdot \phi \cdot \rho_{bf} \cdot \sqrt{\frac{\sigma_B \cdot T}{\rho_{np} \cdot d_{np}}} \cdot f(T, \phi). \tag{13}$$

In which, d_{np} is represented by the nanotube diameter in the nanofluids. The thermophysical properties of the base fluid and nanoparticles were conducted at a reference temperature of 30 °C (Table 3).

2.4 Governing equation

This numerical CFD simulation involved fluid flow and heat transfer processes under a steady state. The incompressible flow was modeled using the steady-state assumption. Governing equations were required for the numerical domain: mass, momentum, and energy conservation (Taylor 2011) for heat transmission through convection in the microchannel. The equation may be expressed as a tensor, as seen below.

Conservation of mass:

$$\frac{\partial \rho_f}{\partial t} + \frac{\partial \rho_f u_i}{\partial x_i} = 0. \tag{14}$$

Conservation of momentum:

$$\rho_f \frac{\partial u_i}{\partial t} + \rho_f \frac{\partial u_i}{\partial x_j} = -\frac{\partial p}{\partial x_i} + \rho_f g_i + \frac{\partial}{\partial x_j} \left(\mu_f \frac{\partial u_i}{\partial x_j} \right) + \frac{\partial}{\partial x_j} \left(\mu_f \frac{\partial u_j}{\partial x_i} \right) - \frac{2}{3} \frac{\partial}{\partial x_j} \left(\mu_f \frac{\partial u_k}{\partial x_k} \right) = 0. \tag{15}$$

Table 3 Thermophysical properties of working fluid (Gómez-Villarejo et al. 2019)

Thermophysical properties	Water	BNNTs	Triton X-100
Density (kg m ⁻³)	998.2	1396.6	1070
Dynamic viscosity μ (Pa s)	0.001	1.72×10^5	0.027
Thermal conductivity k (W m ⁻¹ K ⁻¹)	0.60	46	0.252
Specific heat C_p (J kg ⁻¹ K ⁻¹)	4182	1225	2415

Conservation of energy:

$$\rho_f \frac{\partial h}{\partial t} + \rho_f u_j \frac{\partial h}{\partial x_j} = \frac{\partial p}{\partial t} + u_i \frac{\partial p}{\partial x_i} + \frac{\partial}{\partial x_i} \left(k_f \frac{\partial T_f}{\partial x_i} \right) + \tau_{ij} \frac{\partial u_i}{\partial x_j} \quad (\text{fluid domain}), \tag{16}$$

$$\frac{\partial}{\partial x_i} \left(k_s \frac{\partial T_s}{\partial x_i} \right) = 0 \quad (\text{substrate conduction}). \tag{17}$$

The mathematical formulation requires solving boundary conditions repeatedly in each cell centroid, as presented in Table 4. A homogeneous heat flux (q), 790 W cm^{-2} , was assigned at the bottom wall of the heat sink. It was assumed that this heat flux was homogeneous because the surface area contact between the heat source and the nanofluid consisted of the substrate and t distance between them. Besides, the inlet temperature was varied from 10 to $70 \text{ }^\circ\text{C}$ to investigate the effect of different temperature ranges. In addition, the mass and volume fraction range began from 0.005 to $0.02 \text{ wt.}\%$ and 0.05 to $0.35 \text{ vol.}\%$ experimental validation on the thermal property. It was believed that the majority of exterior walls were completely insulated from the computational domain. The x and z coordinates of the heat sink planes are subjected to symmetrical boundary requirements. The fluid flow rate and the temperature entering the microchannel are $4.7 \text{ cm}^3 \text{ s}^{-1}$ and $30 \text{ }^\circ\text{C}$, respectively.

In contrast, the channel outlet has a constant static pressure barrier condition. The conjugate boundary conditions between fluid and wall energy equations are temperature and heat flow continuity Eqs. (14)–(17) were numerically solved with the aid of Ansys Fluent and a finite volume CFD solver. The simulation was completed when the residual values for all the governing equations used achieved minimum criteria, below 1×10^{-6} with constant error.

2.5 Data acquisition

In this section, the geometrical ratio was represented by the channel aspect ratio, α and wall width ratio, β was fixed throughout this study. The thermal and hydraulic performance and standard dimensionless parameters of the microchannel heat sink (MCHS) were defined below. The geometrical ratio (Shamsuddin et al. 2021) begins with α as seen below:

$$\alpha = \frac{H_c}{W_c}. \tag{18}$$

The channel aspect ratio, α is defined as the ratio of channel height to channel width:

$$\beta = \frac{W_w}{W_c}. \tag{19}$$

The wall width ratio β is represented by the ratio of wall width to channel width. Besides of geometrical ratio, the calculation of thermal resistance (Leng et al. 2015) can be seen below:

$$R_{th} = \frac{\Delta T_{max}}{qA_s}, \tag{20}$$

whereas A_s is the heat flux substratum area, and ΔT_{max} is the maximum heat sink temperature rise defined as,

$$\Delta T_{max} = T_{s,o} - T_{f,i}. \tag{21}$$

The pumping power required to move the fluid flow throughout the microchannel cavity is given below (Shen et al. 2017):

$$\bar{P} = n \cdot u_{avg} \cdot A_c \cdot \Delta p. \tag{22}$$

The pressure drop, Δp , and the average flow velocity, u_{avg} are used to calculate the Reynold number, Re , as below:

$$Re = \frac{\rho u_{avg} D_h}{\mu}. \tag{23}$$

Table 4 Setup of CFD boundary condition

Boundary condition	Value
Analysis type	Steady-state (Hong et al. 2007)
Type of flow	Laminar (Hong et al. 2007)
Number of cycles	400
Ambient and inflow temperature	$30 \text{ }^\circ\text{C}$ (Halefadi et al. 2014)
Inlet flux	$4.7 \text{ cm}^3 \text{ s}^{-1}$ (Halefadi et al. 2014)
Outlet flux	0 Pa
Heat flux	790 W cm^{-2} (Tuckerman and Pease 1981)
Pressure correction type	SIMPLE method (Hong et al. 2007)

The Reynold number represents the ratio of inertial force to viscous force. ρ is density, μ is the absolute viscosity, and D_h is the hydraulic diameter given as below:

$$D_h = \frac{2H_c W_c}{H_c + W_c}. \quad (24)$$

The Nusselt number (Nu) represents the ratio of thermal convection to the thermal conductivity of the nanofluid, as represented below:

$$\text{Nu} = \frac{hD_h}{k}, \quad (25)$$

where h is convection heat transfer and k is conduction heat transfer.

2.6 Boundary conditions

2.6.1 Inlet boundary condition of a microchannel

Assumption of laminar flow was used throughout the study since the Reynold number was below 700. Therefore, the inlet velocity is defined as below:

$$V_{\text{inlet}} = \frac{\dot{m}}{\rho A_s}. \quad (26)$$

The cross-sectional area represented by A_s and the mass flow rate of the fluid is represented with \dot{m} .

2.6.2 Outlet boundary condition

Static pressure is assigned outlet section of the microchannel heat sink. The static pressure is assumed to be atmospheric pressure.

2.6.3 Wall boundary condition

On the inside—channel wall of the microchannel heat sink, a no-slip condition for fluid flow was imposed. In addition, an adiabatic condition was assigned to the top portion of the microchannel to ensure the direct effect of heat losses from convective heat transfer of fluid flow.

2.7 Mesh sensitivity test

This study employed the finite volume method to solve the solution iteratively. The accuracy of the solution relies on the size of the mesh. The smallest mesh provided the highest accuracy. However, the situation may increase the computational load and lengthen the time required. As a result, selecting the optimal mesh size strikes a balance between solution accuracy and low computational load. In addition, mesh refinement between solid and fluid layers needs

to be defined to capture viscous sublayer flow region with y^+ less than 5 (Singh et al. 2017). Therefore, the model utilized a growth rate of 1.2, and the first mesh thickness near the wall was 0.005 mm. After the first layer thickness was established, a mesh sensitivity test was conducted to provide the highest mesh accuracy (Mat et al. 2020, 2021a, b). In this test, ten different meshes were generated. That generated mesh was identified as representative cell length. The representative cell length is the ratio of mesh size over characteristic length. In the case of a microchannel, the characteristic length is 1 cm. Three meshes were chosen as coarse, medium, and fine meshes from the generated meshes to begin with the first trial. The process was repeated several times until the value of extrapolated error was less than 5%. The extrapolated error is the relative difference between an extrapolated solution and a numerical solution. The extrapolated value was calculated using the Richardson Extrapolation method (Roache and Knupp 1993). Based on the generated result, as shown in Fig. 2, the selected optimum representative cell length that gives acceptable numerical accuracy is 1.2×10^{-5} . This length was used for the data validation study in the next section.

2.8 Validation study

This study employed a water-based working fluid to validate the computational domain of the microchannel geometry. The range of Reynold numbers, from 200 to 800, justified the behavior in a computational domain. The numerical simulation measured thermal resistance, as shown in Fig. 3 and pressure drop, as presented in Fig. 4, over different Reynold numbers (Re). Based on Fig. 3, the relative error increases with an increase of Re. The reason was probably due to viscous-sub layer approximation error as the value depends on

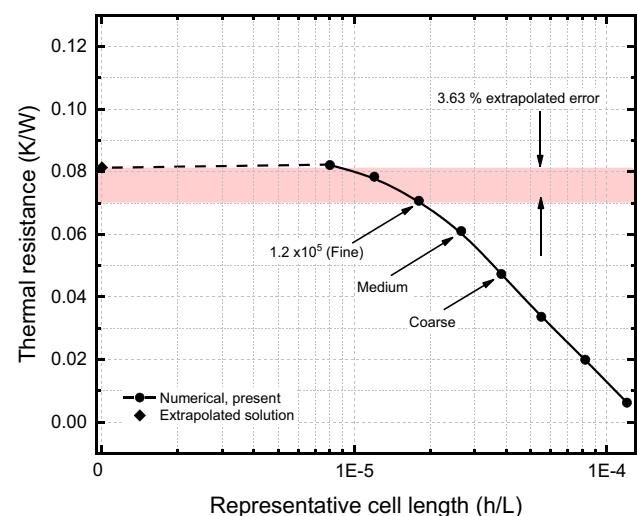


Fig. 2 Mesh sensitivity test

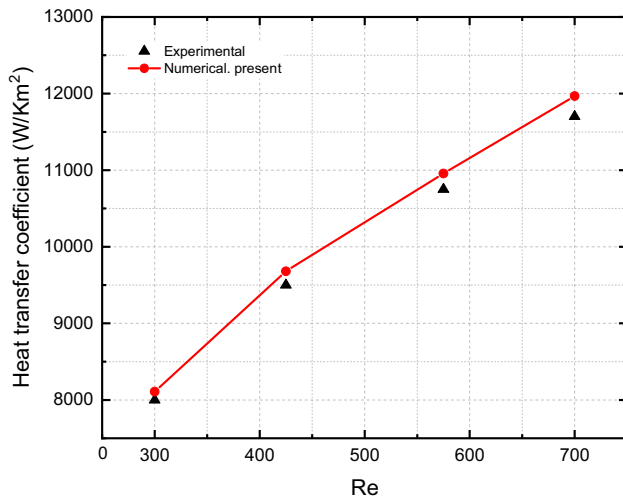


Fig. 3 Validation of heat transfer coefficient

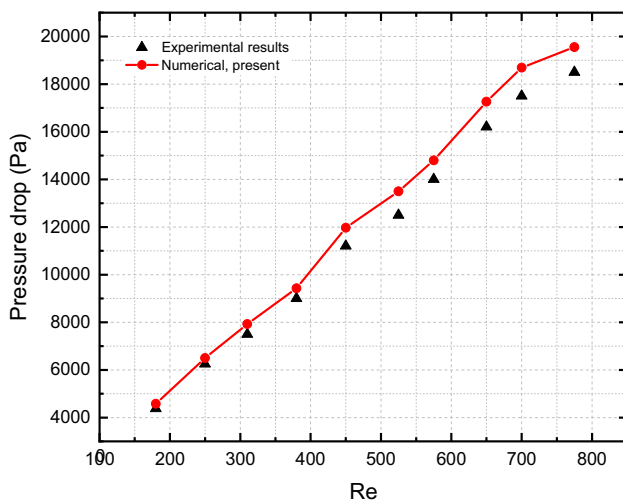
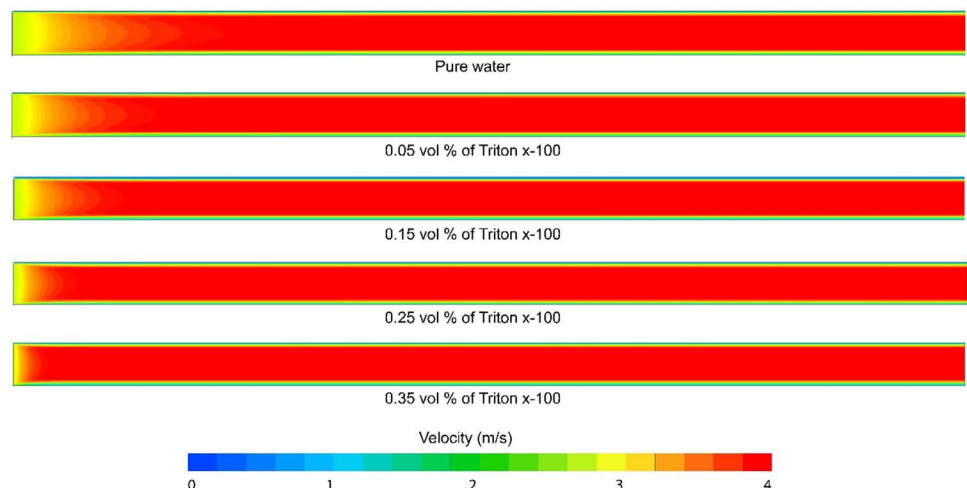


Fig. 4 Validation on pressure drop

Fig. 5 Velocity contour plot for different TX-100 volume fractions



flow velocity. From the graph, the maximum relative error is around 5% at Re of 700. In addition to comparing the heat transfer coefficient, the second parameter, pressure drop, was validated numerically, as shown in Fig. 4. Based on the graph, the relative errors increase with Re increases, and the numerical simulation value over-predicted the experimental result (Lee and Mudawar 2007). Based on the graph, the maximum relative error is approximately 4% at Re of 800. The numerical computation solution was therefore promised for this study based on the data validation study.

3 Result and discussion

With numerical accuracy confirmed, thermal and hydraulic performance effects were investigated on different surfactant volume fractions, nanoparticle mass fractions and nanotube diameter against pure water. In particular, those performances were analyzed on a specific range of Re and temperature 300–700 and 10–70 °C, respectively. These ranges were selected for comparison with the previous review of the literature. This section introduces the flow pattern to enhance comprehension of the interaction and interpretation of the flow.

3.1 Flow pattern

The inlet velocity inside the microchannel heat sink (MCHS) increases with the increment of volume fraction, as presented in Fig. 5. The reason is that adding more volume fractions will increase the fluid viscosity, directly related to Eq. (23). As a result, fluid moves with lower velocity. Lower velocity may cause a long entrance as the fluid takes time to develop. The development flow can be seen in Fig. 6. In the figure, velocity streamline start to develop after the fully develop flow as shown in the inlet section. Pure water

Fig. 6 Velocity streamline for different TX-100 volume fractions

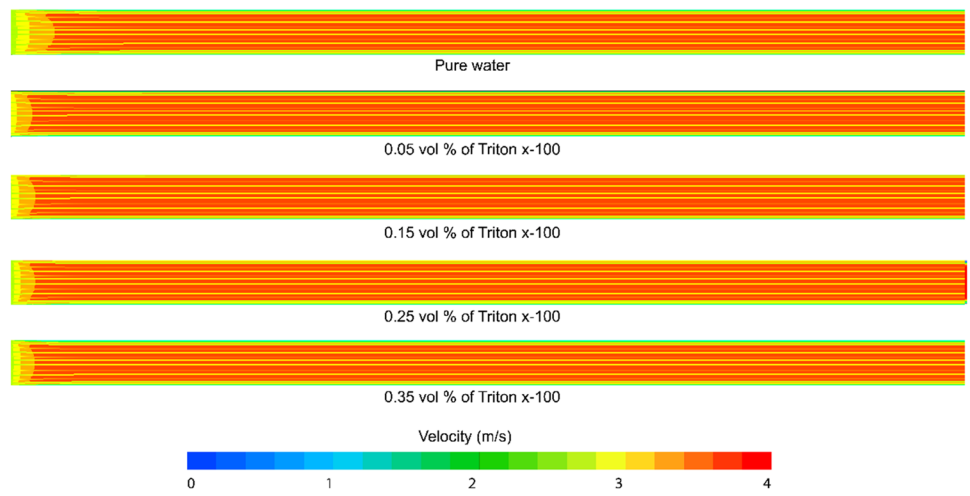


Fig. 7 Temperature contour plot for different TX-100 volume fractions

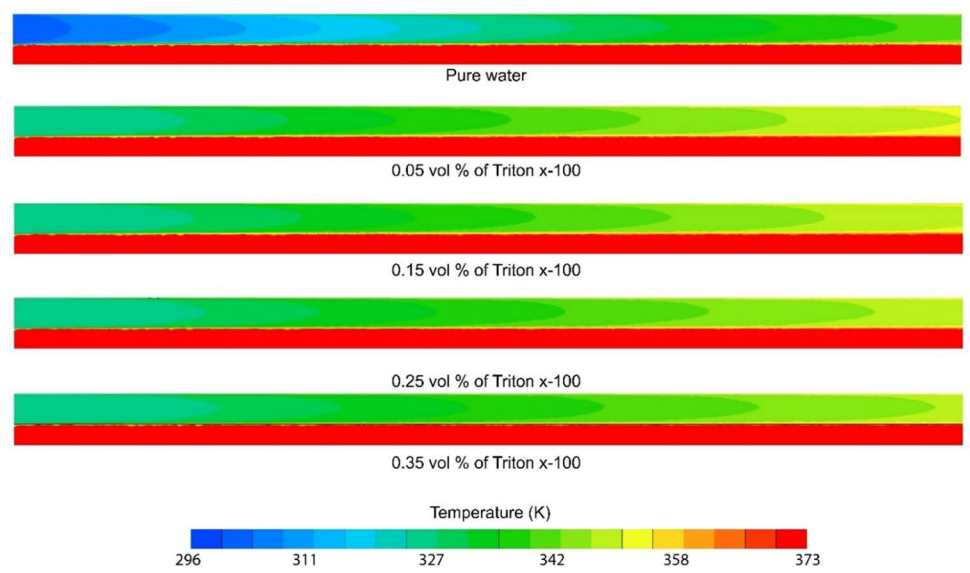


Fig. 8 Total pressure contour plot for different TX-100 volume fractions

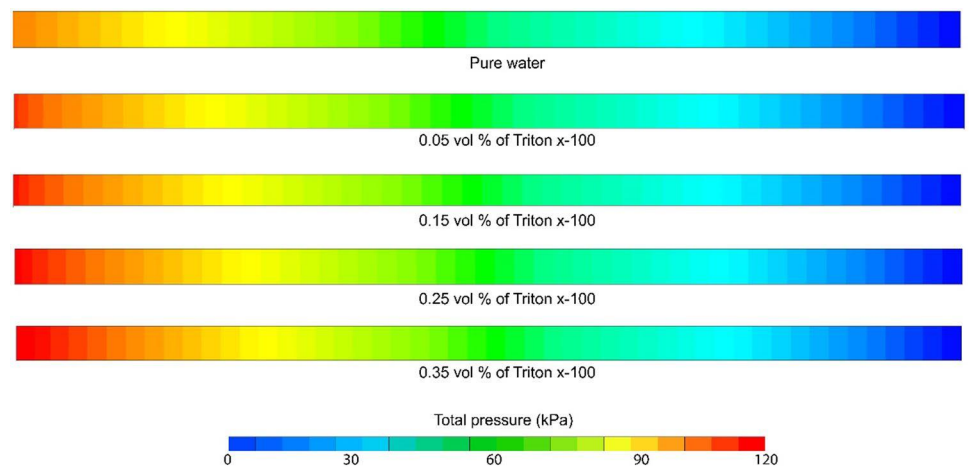


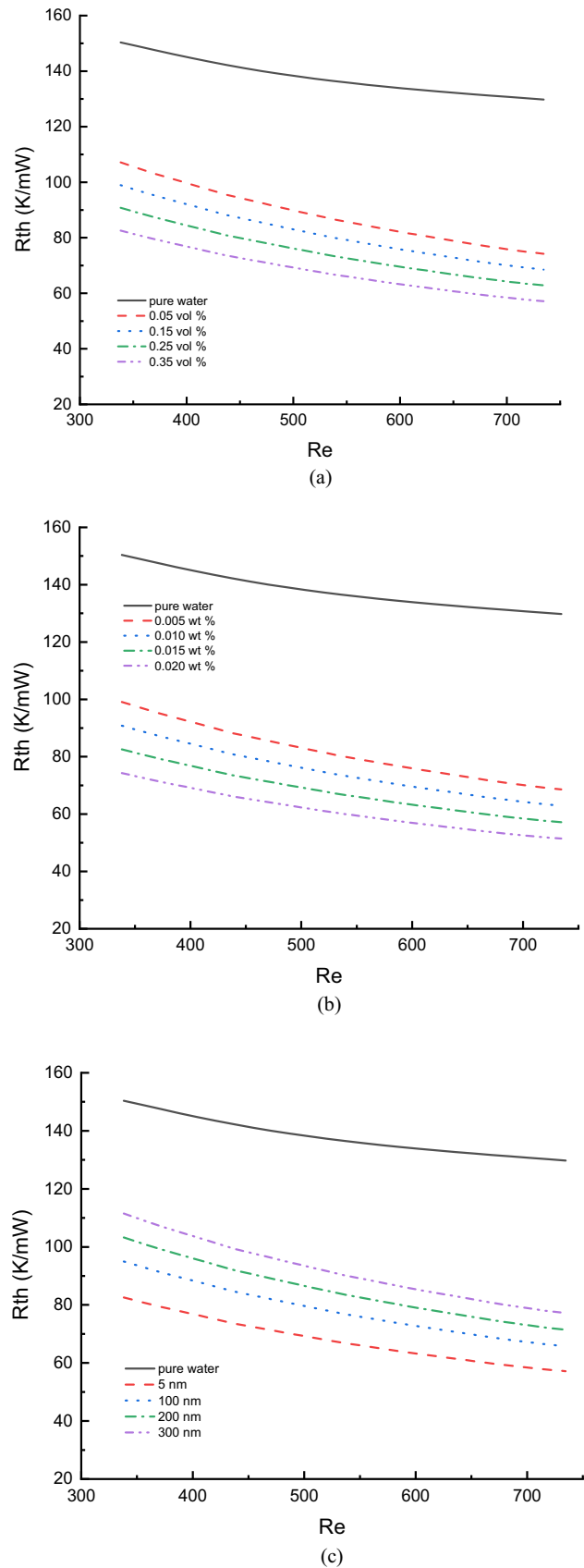
Fig. 9 Effects of thermal resistance on Re with different of **a** TX-100 surfactant volume fraction, **b** BNNT nanoparticle mass fraction, and **c** size of nanoparticle diameter

alone has the largest entrance length, reflecting the delay in flow development. The delay in flow development affects the time for heat absorption by convective heat transfer. In addition, the velocity streamlines embedded in the same velocity contour plot demonstrate that the velocity streamlines of the wall are close to each other for all volume fraction ranges. Figure 7 presents the temperature distribution inside the microchannel heat sink. Flow development plays a crucial role in the effective heat enhancement process. At the flow entrance, fluid begins to absorb the heat as compared to pure water alone. Incorporating nanoparticles and stabilizing them with a surfactant facilitates the even distribution of heat from the entrance to the outlet section. Apart from that, pressure distribution along the channel can be shown in Fig. 8. As expected, the lowest pressure can be seen at the channel's entrance for the pure water, while the base fluid with surfactant and nanotubes contributed to the largest pressure drop in the channel. This is due to the fact that pure water has a lower viscosity than nanofluid. Consequently, this affected the pressure drop. For accurate data interpretation, additional research was required to analyze the effect of thermal and hydrodynamic performance.

3.2 Thermal performance

3.2.1 Thermal resistance

Thermal resistance inside the microchannel heat sink (MCHS) increases with the Re in all cases, as seen in Fig. 9. Additional Triton TX-100 surfactant and Boron Nitride nanoparticle in nanofluid leads to better heat transfer enhancement. This is likely due to the additional substances that act as heat carriers to distribute heat throughout the MCHS cavity evenly. Due to the dispersion functionality of these substances, the nanofluid's heat transfer performance is enhanced. Hence, the usage of nanofluid and surfactant in a base fluid is increasing for better heat thermal management. It is also expected that the demand for these substances continues to grow along with complex advancements in the heat transfer process and higher heat flux capacity, which water alone is unable to sustain. Due to the superiority of this substance, further investigations was conducted to determine the effect of varying concentrations of these substances: nanofluid, surfactant, and the size of nanotube diameter. Increasing surfactant concentration in the nanofluid reduced the thermal resistance in the microchannel heat sink. The maximum drop in the thermal resistance with the other surfactant concentration was reported at approximately 90% as a reference of the pure water for 0.35 vol% surfactant



across all the Re , as seen in Fig. 9a. In contrast, the lowest surfactant concentration contributes less thermal resistance to the microchannel. The reason is that the nanofluid obtains stability because surfactant effect (Khairul et al. 2016). This additional surfactant prevents the nanoparticle from particle agglomeration as it acts as anti-surface tension between particle to particle. Figure 8b presents the effect of nanoparticle concentration ranging between 0.005 to 0.02 wt.% with an increment of 0.005 wt.%. The thermal resistance was reduced with a further increase in nanoparticle mass fraction. The maximum drop for thermal resistance was twice as compared with the pure water for 0.02 wt.% for all ranges of the Re , as demonstrated in Fig. 9b. Despite this, the smallest nanoparticle concentration gives the lowest drop in the thermal resistance, around 50% for 0.005 wt.%. This additional nanoparticle concentration enhances the heat transfer process as a result of the solid nanoparticles' enhanced conductivity. These nanoparticles absorb heat and evenly distribute it throughout the fluid (Jebasingh and Arasu 2020). The effects of thermal resistance on nanoparticle diameters ranging from 5 to 300 nm are depicted in Fig. 9c. Reportedly, the introduction of nanoparticles of varying sizes improved the microchannel's heat transfer process significantly. The small size of the nanoparticle reduces the thermal resistance by as much as twice as compared to pure water alone. This is due to increased surface area contact between particles for better heat conductivity (Ealia and Saravanakumar 2017). Figure 10 presents the effects of thermal resistance on temperature with various concentrations of nanotubes in the base fluid. As expected, the thermal resistance increases as the inlet fluid temperature rises for all cases, as shown in Fig. 10a. The correlation also can be seen in Eq. (20). The significant finding reveals that the maximum dropping in the thermal resistance was around 75% for 0.35 vol.% surfactant concentration as a reference to pure water across all ranges of temperature. This may be due to the specific heat capacity of the nanofluid. As indicated in Eq. (20) following Eq. (21), these equations illustrate that the thermal resistance increase with an increased temperature difference between the wall and fluid temperature. Figure 10b demonstrates the effect of thermal resistance on temperature with different mass fractions of the nanoparticle. The critical finding reveals that the lowest temperature of nanofluid contributes the lowest thermal resistance, approximately around 70 K mW^{-1} for 0.005 wt.% at 10°C , as shown in Fig. 10b. At the same time, the lowest thermal resistance for different sizes of nanoparticles was reported at around 80 K mW^{-1} for 0.005 wt.% at 10°C , as seen in Fig. 10c. However, the concentration effects of the surfactant and nanofluid are quite complex. As shown in Fig. 10a, b, pure water appears to be more advantageous than adding these substances for minimizing thermal resistance at temperatures below 303 K. Due to the negligible effect of those concentrating substances on thermal performance,

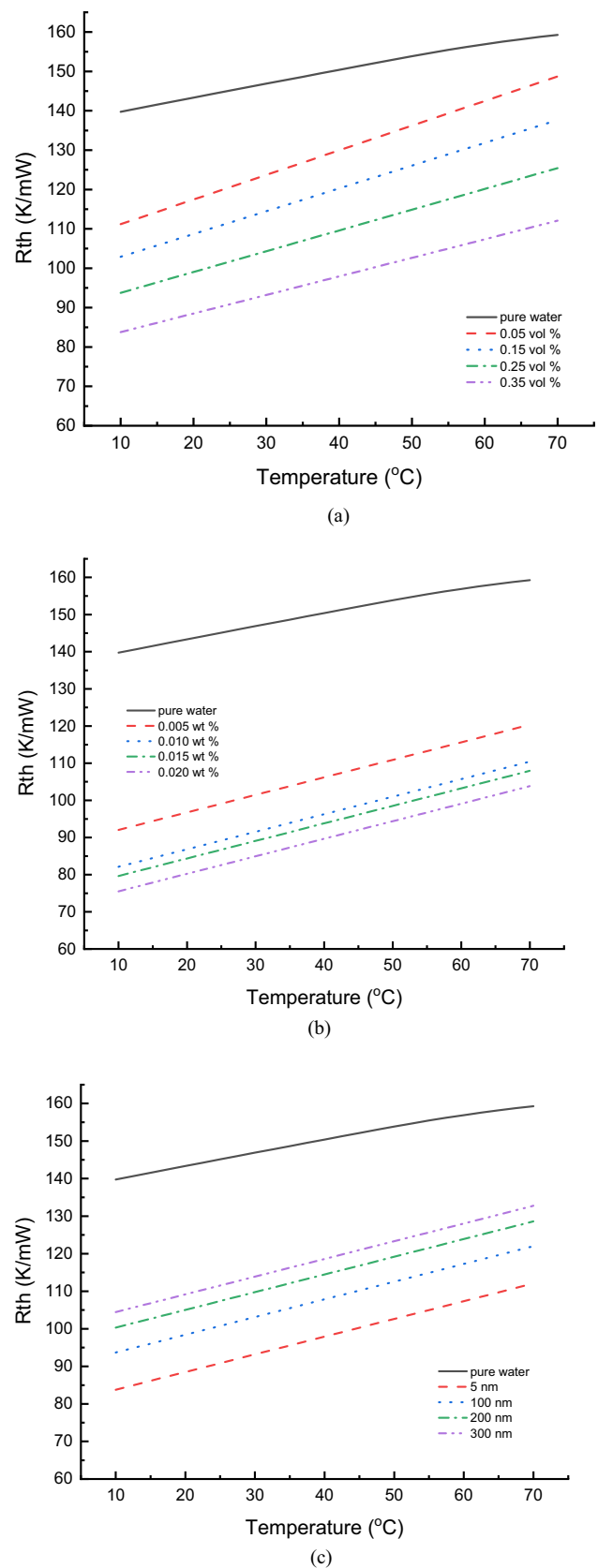


Fig. 10 Effects of thermal resistance on temperature with different of **a** TX-100 surfactant volume fraction, **b** BNNT nanoparticle mass fraction, and **c** size of nanoparticle diameter

all concentrations provide up to 24 and 12% more thermal resistance than water alone at 280 and 290 K, respectively. At temperatures greater than 303 K, however, different concentrations of these substances significantly reduce thermal resistance compared to pure water. Therefore, it can be concluded that modifying the concentration of the surfactant, the nanofluid, and the diameter of the nanofluid provides optimal thermal conditions for improving MCHS.

3.2.2 Nusselt number

An additional parameter for the thermal performance, Nusselt number (Nu), was introduced in this section. This Nu is a crucial parameter in investigating the ratio of convection heat transfer to conduction heat transfer for the nanofluid, as indicated in Eq. (25). Increasing the Reynold number (Re) increases the Nu for all the cases. This is due to the majority of heat convection as opposed to the conductivity of heat transfer, as indicated by Eq. (25). Increasing flow velocity translates to frequency contact of fluid flow to the heat source. Thus, the heat transfer enhancement process (Esfe et al. 2018). Besides, the trend of different surfactant concentrations on Nu, as shown in Fig. 11a, seems quite complicated. For instance, the surfactant volume fraction of 0.35 vol.% gave the lowest Nu as compared to other concentrations for the Re below 350. While after that point, the Nu for 0.35 vol.% increase more than other surfactant concentrations. However, significant finding reveals that 0.05 vol.% provides the lowest Nu as compared to others concentration and even lower than that the pure water. At the same time, the surfactant concentration that is comparable to pure water is 0.15 vol.% as the Nu characteristic is almost similar after the Re of 450. Figure 11b also seems to have a complex trend as the value of Nu contradicts before the Re of 400. The critical finding shows that a lower mass fraction of 0.005 wt.% provides a better heat transfer process than other mass fractions after the Re of 400. The lowest Nu was reported for the highest nanoparticle mass fraction of 0.02 wt.%. This finding is essential for evaluating the amount of nanoparticle concentration as this influences not only the Nu number but also thermal resistance performance. Figure 11c demonstrates the effect of different sizes of nanoparticles in nanofluid on the Nu. The result shows an increasing size of nanoparticles will enhance the convection heat transfer process and the Nu as well. This is likely due to the contribution of the smallest nanoparticles to the greatest number of nanoparticles that increase the thermal conductivity of the fluid. Thus, Eq. (25) indicates that the thermal conductivity is inversely proportional to the Nu. The effect of Nu against inlet flow temperature is highly responsible at around 20 °C, as shown in Fig. 12. In addition, the effect of surfactant concentration in the nanofluid shows that increasing the surfactant concentration gives the highest Nu

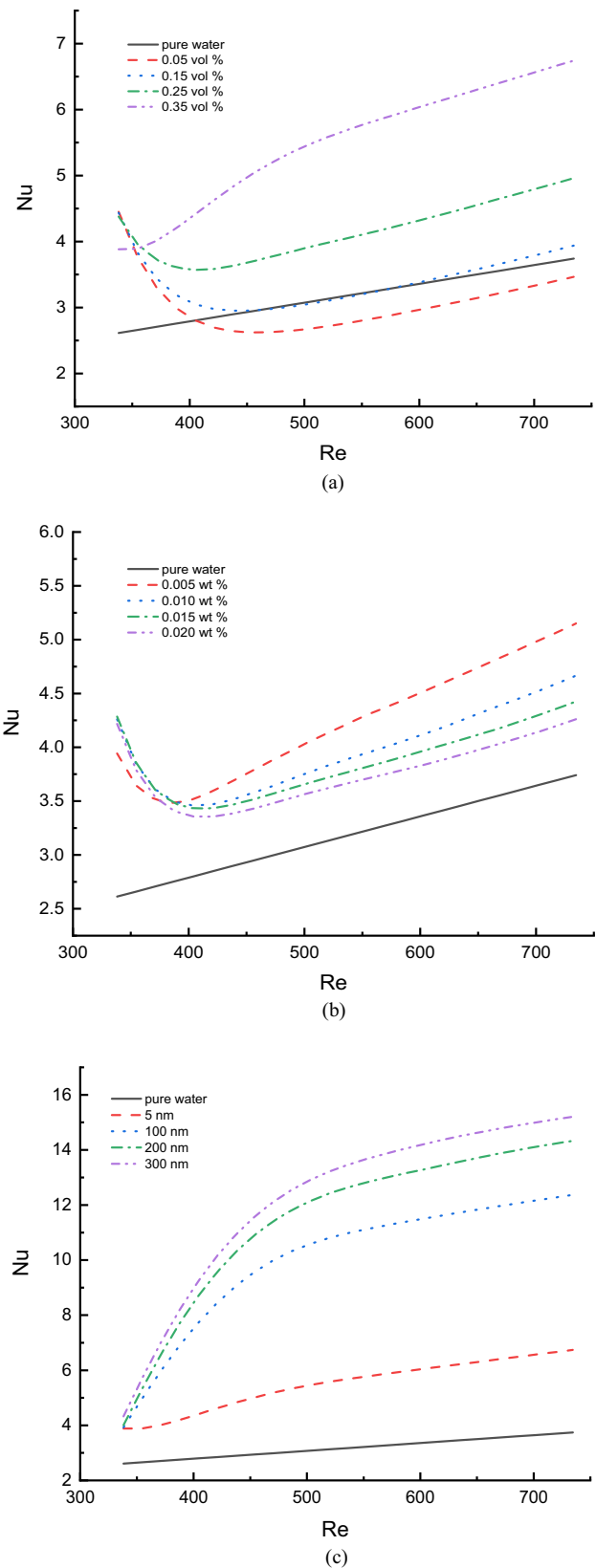


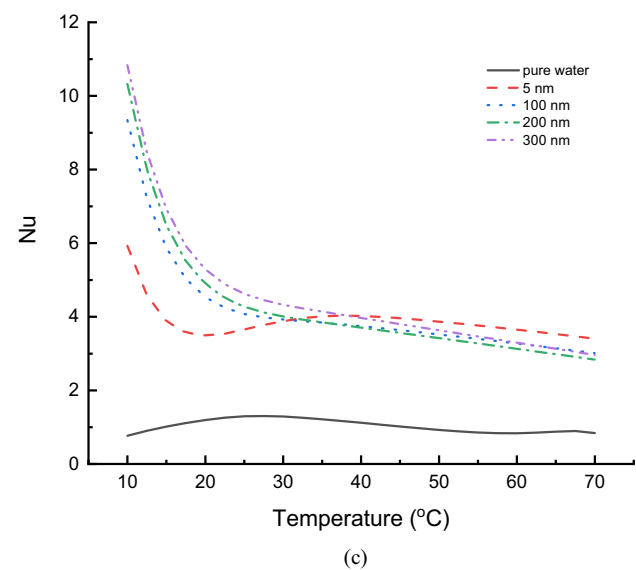
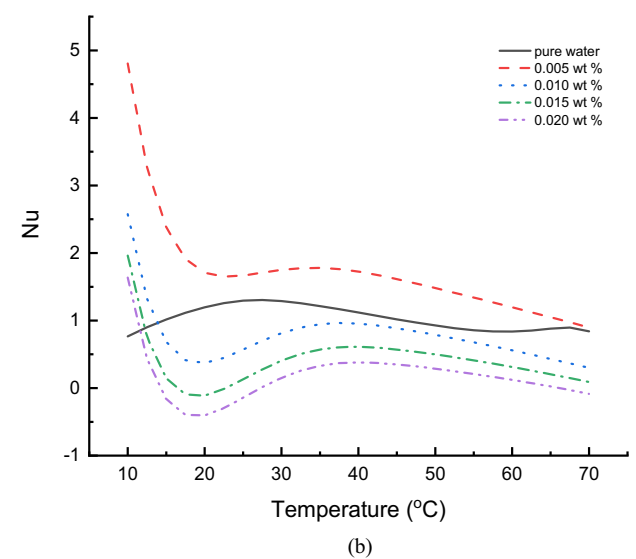
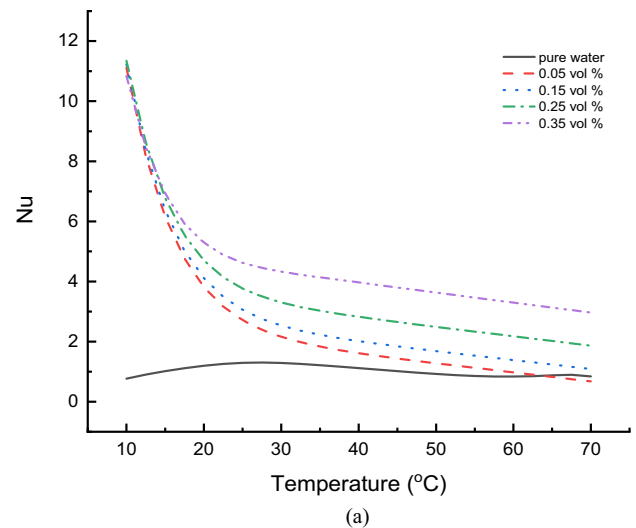
Fig. 11 Effects of Nusselt number on Reynold number for different **a** TX-100 surfactant volume fraction, **b** BNNT nanoparticle mass fraction, and **c** size of nanoparticle diameter

Fig. 12 Effects of Nusselt number on temperature for different **a** TX-100 surfactant volume fraction, **b** BNNT nanoparticle mass fraction, and **c** size of nanoparticle diameter

in the microchannel. Furthermore, adding a small amount of surfactant concentration still gives a better thermal performance as a reference to the pure water alone, as presented in Fig. 12a. However, this is not the case for adding nanoparticle mass fraction into the nanofluid. The result shows that the least amount of nanoparticle mass, 0.005 wt.% contribute to the highest Nu and above the pure water. The rest of the mass fraction ranged from 0.01 to 0.02 wt.% gives the lowest Nu even less than the pure water, as shown in Fig. 12b. Figure 12c illustrates the influence of nanoparticle size on the Nu as a function of temperature. Changes in particle size have a substantial effect on the thermal performance of a microchannel. However, significant finding revealed that at the lowest temperature, the biggest nanoparticle has the largest nanoparticle size. It seems that the trend for the smallest particle size, 5 nm overperforms the Nu as compared to the rest of the nanoparticle size at 40 °C.

3.3 Pressure drop

The effects of pressure drop against Reynold number (Re) are presented in Fig. 13. Almost linearly, increasing Re will increase the pressure drop for all cases. This is because the Re is influenced by fluid flow velocity, as shown in Eq. (23). This velocity directly correlates with the pumping power and pressure drop, as indicated in Eq. (22). From this equation, increasing Re will increase the velocity leading to more pumping power requirement. In this instance, more pumping power is required because the fluid flow is traveling at a high velocity, resulting in increased friction across the MCHS channel. Since reducing pumping power is one of the keys to improving the MCHS, selecting proper Re might have a better effect on reducing energy consumption during operation. It is also suggested that lowering fluid flow velocity inside MCHS might have a dual effect in enhancing the performance of MCHS in terms of lowering both pressure drop and thermal resistance. However, it is observed that adding additional Boron Nitride Nanotube (BNNT) and Triton TX-100 surfactant increases the pressure drop marginally. In turn, this will necessitate increased pumping capacity for these substances. The reason is that these additional substances increase fluid viscosity. As seen in Eq. (23), the fluid velocity directly depends on fluid viscosity. Increasing fluid viscous will impede the fluid motion, thus resulting in more pressure drop as indicated in Eq. (22), in which velocity is inversely proportional to pressure drop. Since the additional nanotube and surfactant will cause a pressure drop, further investigation is required to understand whether different concentrations can minimize the pressure drop. Figure 13a



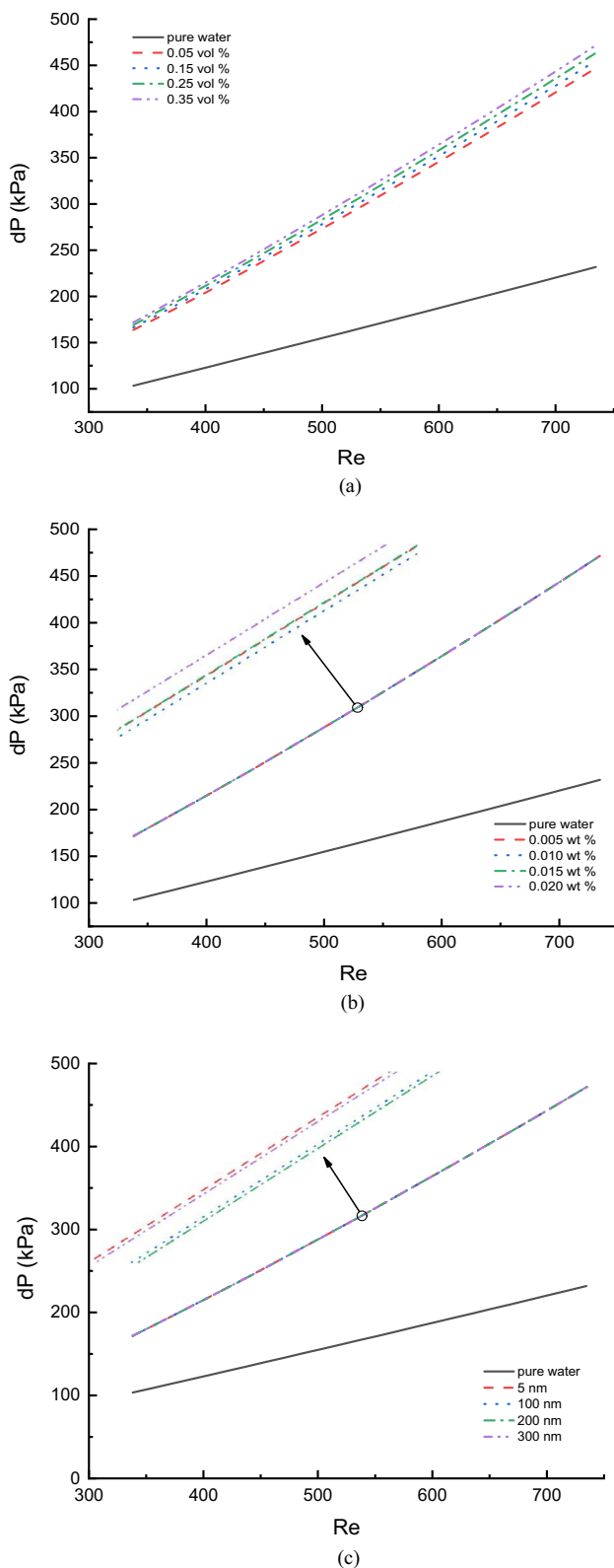


Fig. 13 Effects of pressure drop on Reynold number with different of **a** TX-100 surfactant volume fraction, **b** BNNT nanoparticle mass fraction, and **c** size of nanoparticle diameter

demonstrates pressure drop against Re with different volume fractions of the surfactant. As anticipated, adding more volume fraction of the surfactant in the nanofluid will increase the pressure drop. This is because the base fluid receives more fluid density and viscosity. In turn, this will increase the pressure drop, as previously explained, necessitating greater pumping power to move the fluid. However, the choice of volume fraction should be carefully considered, as adding less surfactant may provide an advantage in minimizing pressure drop, but destabilize the nanotube. That would affect the increase of thermal resistance, as explained in Fig. 8a. However, the trend for Fig. 13b, c seem insignificant for varying the mass fraction and the nanotube size. However, additional surfactant and nanotubes have increased pressure drop by 75% at Re of 350 and 125% at Re of 700.

4 Conclusion

In the present study, a numerical CFD method was adopted to investigate two objectives: the flow pattern and heat transfer performance of a microchannel heat sink containing Boron Nitride nanotubes (BNNT) and Triton X-100. Significant findings following the two objectives revealed that surfactant TX-100 inside nanofluid reduced the fully develop flow length compared to pure water alone. The pure water took more time to achieve a fully developed flow inside the microchannel heat sink cavity. The thermal resistance drops as much as 90% compared to pure water with a surfactant concentration of 0.35 vol.% and adding 0.02 wt.% especially at a low Reynold number (Re) of 400. It was discovered that the Nusselt number (Nu) increased twice from the pure water with additional 0.35 vol.% of surfactant after Re of 400. The biggest nanotube size has increased the Nu with the Re. The pressure drop appears to be a drawback for the nanofluid with surfactant implementation in the microchannel when additional surfactant and nanotubes are added to enhance thermal performance. However, additional surfactant and nanotubes have increased pressure drop by 75% at Re of 350 and 125% at Re of 700.

Acknowledgements This research was sponsored by the Ministry of Higher Education (MOHE) through Fundamental Research Grant Scheme (FRGS/1/2021/TK0/UTM/02/98).

Declarations

Conflict of interest The authors have no competing interests to declare that are relevant to the content of this article.

References

- Alfaryjat A, Mohammed H, Adam NM, Stanciu D, Dobrovicescu A (2018) Numerical investigation of heat transfer enhancement using various nanofluids in hexagonal microchannel heat sink. *Therm Sci Eng Prog* 5:252–262
- Alhamid M, Nasruddin N, Susanto E, Vickary T, Budiyanto M (2019) Refrigeration cycle exergy-based analysis of hydrocarbon (r600a) refrigerant for optimization of household refrigerator. *Evergreen* 6(1):71–77
- Ardiansyah SR, Orlando AM, Rahman A, Prihantini NB (2019) Tubular photobioreactor: a preliminary experiment using *Synechococcus* sp. (cyanobacteria) cultivated in NPK media for biomass production as biofuel feedstock. *Evergreen* 6(2):157–161
- Babu JR, Kumar KK, Rao SS (2017) State-of-art review on hybrid nanofluids. *Renew Sustain Energy Rev* 77:551–565
- Bahiraei M, Monavari A (2020) Impact of nanoparticle shape on thermohydraulic performance of a nanofluid in an enhanced microchannel heat sink for utilization in cooling of electronic components. *Chin J Chem Eng* 40(12):36–47
- Bahiraei M, Heshmatian S, Goodarzi M, Moayedi H (2019) CFD analysis of employing a novel ecofriendly nanofluid in a miniature pin fin heat sink for cooling of electronic components: effect of different configurations. *Adv Powder Technol* 30(11):2503–2516
- Bahiraei M, Mazaheri N, Daneshyar MR (2021) Employing elliptical pin-fins and nanofluid within a heat sink for cooling of electronic chips regarding energy efficiency perspective. *Appl Therm Eng* 183:116159
- Choi TJ, Jang SP, Kedzierski M (2018) Effect of surfactants on the stability and solar thermal absorption characteristics of water-based nanofluids with multi-walled carbon nanotubes. *Int J Heat Mass Transf* 122:483–490
- Chuan L, Wang X-D, Wang T-H, Yan W-M (2015) Fluid flow and heat transfer in microchannel heat sink based on porous fin design concept. *Int Commun Heat Mass Transfer* 65:52–57
- Dey D, Kumar P, Samantaray S (2017) A review of nanofluid preparation, stability, and thermo-physical properties. *Heat Transf Asian Res* 46(8):1413–1442
- Drummond KP, Back D, Sinanis MD, Janes DB, Peroulis D, Weibel JA, Garimella SV (2018) A hierarchical manifold microchannel heat sink array for high-heat-flux two-phase cooling of electronics. *Int J Heat Mass Transf* 117:319–330
- Ealia SAM, Saravanakumar M (2017) A review on the classification, characterization, synthesis of nanoparticles and their application. In: Paper presented at the IOP conference series: materials science and engineering
- Esfé MH, Nadooshan AA, Arshi A, Alirezaie A (2018) Convective heat transfer and pressure drop of aqua based TiO₂ nanofluids at different diameters of nanoparticles: data analysis and modeling with artificial neural network. *Physica E* 97:155–161
- Fisher TS, Torrance KE (2001) Optimal shapes of fully embedded channels for conjugate cooling. *IEEE Trans Adv Packag* 24(4):555–562
- Ghani IA, Sidik NAC, Mamat R, Najafi G, Ken TL, Asako Y, Japar WMAA (2017) Heat transfer enhancement in microchannel heat sink using hybrid technique of ribs and secondary channels. *Int J Heat Mass Transf* 114:640–655
- Ghasemi B, Aminossadati S (2010) Brownian motion of nanoparticles in a triangular enclosure with natural convection. *Int J Therm Sci* 49(6):931–940
- Ghorabae H, Emami MRS, Shafahi M (2020) Effect of nanofluid and surfactant on thermosiphon heat pipe performance. *Heat Transf Eng* 41(21):1829–1842
- Gómez-Villarejo R, Aguilar T, Hamze S, Estellé P, Navas J (2019) Experimental analysis of water-based nanofluids using boron nitride nanotubes with improved thermal properties. *J Mol Liq* 277:93–103
- Gong L, Li Y, Bai Z, Xu M (2018) Thermal performance of microchannel heat sink with metallic porous/solid compound fin design. *Appl Therm Eng* 137:288–295
- Halelfadl S, Adham AM, Mohd-Ghazali N, Maré T, Estellé P, Ahmad R (2014) Optimization of thermal performances and pressure drop of rectangular microchannel heat sink using aqueous carbon nanotubes based nanofluid. *Appl Therm Eng* 62(2):492–499
- Heidarshenas A, Azizi Z, Peyghambarzadeh S, Sayyahi S (2021) Experimental investigation of heat transfer enhancement using ionic liquid-Al₂O₃ hybrid nanofluid in a cylindrical microchannel heat sink. *Appl Therm Eng* 191:116879
- Hong F, Cheng P, Ge H, Joo GT (2007) Conjugate heat transfer in fractal-shaped microchannel network heat sink for integrated microelectronic cooling application. *Int J Heat Mass Transf* 50(25–26):4986–4998
- Husain A, Kim K-Y (2008) Optimization of a microchannel heat sink with temperature dependent fluid properties. *Appl Therm Eng* 28(8–9):1101–1107
- Japar WMAA, Sidik NAC, Mat S (2018) A comprehensive study on heat transfer enhancement in microchannel heat sink with secondary channel. *Int Commun Heat Mass Transf* 99:62–81
- Jebsingh BE, Arasu AV (2020) A comprehensive review on latent heat and thermal conductivity of nanoparticle dispersed phase change material for low-temperature applications. *Energy Storage Mater* 24:52–74
- Khairul M, Shah K, Doroodchi E, Azizian R, Moghtaderi B (2016) Effects of surfactant on stability and thermo-physical properties of metal oxide nanofluids. *Int J Heat Mass Transf* 98:778–787
- Kiliç F, Menlik T, Sözen A (2018) Effect of titanium dioxide/water nanofluid use on thermal performance of the flat plate solar collector. *Sol Energy* 164:101–108
- Knight RW, Hall DJ, Goodling JS, Jaeger RC (1992) Heat sink optimization with application to microchannels. *IEEE Trans Compon Hybrids Manuf Technol* 15(5):832–842
- Lee J, Mudawar I (2007) Assessment of the effectiveness of nanofluids for single-phase and two-phase heat transfer in microchannels. *Int J Heat Mass Transf* 50(3–4):452–463
- Leng C, Wang X-D, Wang T-H, Yan W-M (2015) Optimization of thermal resistance and bottom wall temperature uniformity for double-layered microchannel heat sink. *Energy Convers Manag* 93:141–150
- Li X, Zhu D, Wang X, Wang N, Gao J, Li H (2008) Thermal conductivity enhancement dependent pH and chemical surfactant for Cu–H₂O nanofluids. *Thermochim Acta* 469(1–2):98–103
- Mat MNH, Asmuin NZ, Basir MFM, Goodarzi M, Abd Rahman MF, Khairulfuaad R et al (2020) Influence of divergent length on the gas-particle flow in dual hose dry ice blasting nozzle geometry. *Powder Technol* 364:152–158
- Mat MNH, Asmuin NZ, Basir MFM, Abbas T, Kasihmuddin MSM, Goodarzi M (2021a) Influence of nozzle area ratio on the gas-particle flow for single-hose dry ice blasting nozzle. *J Therm Anal Calorim* 143(3):2343–2354
- Mat MNH, Asmuin NZ, Basir MFM, Safaei MR, Kasihmuddin MSM, Khairuddin TKA, Godarzi M (2021b) Optimizing nozzle convergent angle using central composite design on the particle velocity and acoustic power level for single-hose dry ice blasting nozzle. *J Therm Anal Calorim* 144(6):2159–2173
- Monavari A, Jamaati J, Bahiraei M (2021) Thermohydraulic performance of a nanofluid in a microchannel heat sink: Use of different microchannels for change in process intensity. *J Taiwan Inst Chem Eng* 125:1–14
- Murshed S, Leong K, Yang C (2005) Enhanced thermal conductivity of TiO₂—water based nanofluids. *Int J Therm Sci* 44(4):367–373

- Roache PJ, Knupp PM (1993) Completed richardson extrapolation. *Commun Numer Methods Eng* 9(5):365–374
- Shamsuddin HS, Estellé P, Navas J, Mohd-Ghazali N, Mohamad M (2021) Effects of surfactant and nanofluid on the performance and optimization of a microchannel heat sink. *Int J Heat Mass Transf* 175:121336
- Shen H, Jin X, Zhang F, Xie G, Sunden B, Yan H (2017) Computational optimization of counter-flow double-layered microchannel heat sinks subjected to thermal resistance and pumping power. *Appl Therm Eng* 121:180–189
- Singh J, Rudman M, Blackburn H (2017) The effect of yield stress on pipe flow turbulence for generalized Newtonian fluids. *J Non-newton Fluid Mech* 249:53–62
- Taylor MA (2011) Conservation of mass and energy for the moist atmospheric primitive equations on unstructured grids. *Numerical techniques for global atmospheric models*. Springer, Berlin, pp 357–380
- Tuckerman DB, Pease RFW (1981) High-performance heat sinking for VLSI. *IEEE Electron Device Lett* 2(5):126–129
- Wei X, Joshi Y (2003) Optimization study of stacked micro-channel heat sinks for micro-electronic cooling. *IEEE Trans Compon Packag Technol* 26(1):55–61
- Weisberg A, Bau HH, Zemel J (1992) Analysis of microchannels for integrated cooling. *Int J Heat Mass Transf* 35(10):2465–2474
- Xia G, Ma D, Zhai Y, Li Y, Liu R, Du M (2015) Experimental and numerical study of fluid flow and heat transfer characteristics in microchannel heat sink with complex structure. *Energy Convers Manag* 105:848–857
- Yu W, Xie H, Chen L, Li Y (2010) Investigation on the thermal transport properties of ethylene glycol-based nanofluids containing copper nanoparticles. *Powder Technol* 197(3):218–221
- Zhou J, Cao X, Zhang N, Yuan Y, Zhao X, Hardy D (2020) Micro-channel heat sink: a review. *J Therm Sci* 29(6):1431–1462

Publisher's Note Springer Nature remains neutral with regard to jurisdictional claims in published maps and institutional affiliations.

Springer Nature or its licensor holds exclusive rights to this article under a publishing agreement with the author(s) or other rightsholder(s); author self-archiving of the accepted manuscript version of this article is solely governed by the terms of such publishing agreement and applicable law.